Atmos. Chem. Phys. Discuss., https://doi.org/10.5194/acp-2017-684
Manuscript under review for journal Atmos. Chem. Phys.
Discussion started: 28 August 2017

Atmospheric Chemistry and Physics
Open Access
Discussions

Tropical Continental Downdraft Characteristics: Mesoscale Systems versus Unorganized Convection

Kathleen A. Schiro[1] and J. David Neelin[1]

[1]*Department of Atmospheric and Oceanic Sciences, University of California Los Angeles, Los Angeles, CA, USA*

Corresponding Author: Kathleen A. Schiro, Department of Atmospheric and Oceanic Sciences, University of California, Los Angeles, Box 951565, Los Angeles, CA 90095. E-mail: kschiro@atmos.ucla.edu

Abstract

Downdrafts and cold pool characteristics for mesoscale convective systems (MCSs) and isolated, unorganized deep precipitating convection are analyzed using multi-instrument data from the GOAmazon campaign. For both MCSs and isolated cells, there are increases in column water vapor (CWV) observed in the two hours leading the convection and an increase in wind speed, decrease in surface moisture and temperature, and increase in relative humidity coincident with system passage. Composites of vertical velocity data and radar reflectivity from a radar wind profiler show that the downdrafts associated with the sharpest decreases in surface equivalent potential temperature (θ_e) have a probability that increases towards lower levels below the freezing level. Both MCSs and unorganized convection show similar mean downdraft magnitudes and probabilities with height. This is consistent with thermodynamic arguments: if θ_e were approximately conserved following descent, it would imply that a large fraction of the air reaching the surface originates at altitudes in the lowest 2 km, with probability of lower θ_e dropping exponentially. Mixing computations suggest that, on average, air originating at heights greater than 3 km must undergo substantial mixing, particularly in the case of isolated cells, to match the observed cold pool θ_e, likewise implying a low typical origin level. Precipitation conditionally averaged on decreases in surface equivalent potential temperature ($\Delta\theta_e$) exhibits a strong relationship because the largest $\Delta\theta_e$ values are associated with high probability of precipitation. The more physically motivated conditional average of $\Delta\theta_e$ on precipitation levels

Atmos. Chem. Phys. Discuss., https://doi.org/10.5194/acp-2017-684
Manuscript under review for journal Atmos. Chem. Phys.
Discussion started: 28 August 2017

off with increasing precipitation rate, bounded by the maximum difference between surface θ_e and its minimum in the profile aloft. Precipitation values greater than about 10 mm h^{-1} are associated with high probability of $\Delta\theta_e$ decreases. Robustness of these statistics observed across scales and regions suggests their potential use as model diagnostic tools for the improvement of downdraft parameterizations in climate models.

1 Introduction

Convective downdrafts involve complex interactions between dynamics, thermodynamics, and microphysics across scales. They form cold pools, which are evaporatively cooled areas of downdraft air that spread horizontally and can initiate convection at their leading edge (Byers and Braham 1949; Purdom 1976; Wilson and Schreiber 1986; Rotunno et al. 1988; Fovell and Tan 1998; Tompkins 2001; Khairoutdinov and Randall 2006; Lima and Wilson 2008; Khairoutdinov et al. 2009; Boing et al. 2012; Rowe and Houze 2015). The boundary between the cold pool and the surrounding environmental air, known as the outflow boundary or gust front, is the primary mechanism for sustaining multi-cellular deep convection (e.g. Weisman and Klemp 1986). It has also been shown to trigger new convective cells in marine stratocumulus clouds (Wang and Feingold 2009; Terai and Wood 2013) and in trade-wind cumulus (Zuidema et al. 2011; Li et al. 2014). Downdrafts also have implications for new particle formation in the outflow regions, which contribute to maintaining boundary layer CCN concentrations in unpolluted environments (Wang et al. 2016).

Precipitation-driven downdrafts are primarily a result of condensate loading and the evaporation of hydrometeors in unsaturated air below cloud base (e.g. Houze 1993), with evaporation thought to be the main driver (Knupp and Cotton 1985; Srivastava 1987). It was originally suggested by Zipser (1977) that the downdrafts in the convective part of a system, referred to in the literature as convective-scale downdrafts, are saturated and the downdrafts in the trailing stratiform region (referred to as mesoscale downdrafts) are unsaturated. Studies with large-eddy simulations (LES; Hohenegger and Bretherton 2011; Torri and Kuang 2016) indicate, however, that most convective downdrafts are unsaturated, consistent with evidence that the evaporation of raindrops within the downdraft likely does not occur at a sufficient rate to maintain saturation (Kamburova and Ludlam 1966).

Atmos. Chem. Phys. Discuss., https://doi.org/10.5194/acp-2017-684
Manuscript under review for journal Atmos. Chem. Phys.
Discussion started: 28 August 2017

More recently, studies have shown the importance of downdraft parameters in maintaining an accurate simulation of tropical climate in global climate models (GCMs; Maloney and Hartmann 2001; Sahany and Nanjundiah 2008; Del Genio et al. 2012; Langenbrunner and Neelin 2017). Accurate simulation of MCSs in continental regions (Pritchard et al. 2011) was also shown to be sensitive to downdraft–boundary layer interactions, with significantly improved representation of MCS propagation in the central US once such interactions were resolved. Additionally, representing the effects of downdrafts and cold pools in models has been shown to have positive effects on the representation of the diurnal cycle of precipitation (Rio et al. 2009; Schlemmer and Hohenegger 2014).

This study aims to characterize downdrafts in a comprehensive way in the Amazon for both isolated and mesoscale convective systems, and to provide useful guidance for downdraft parameterization in GCMs. Data from the DOE–Brazil Green Ocean Amazon (GOAmazon) campaign (2014–2015; Martin et al. 2016) provides an unprecedented opportunity to evaluate downdraft characteristics in the Amazon with sufficiently large datasets for quantifying robust statistical relationships describing leading order processes for the first time. Relationships explored previously, primarily in tropical oceanic or mid-latitude regions, such as time composites of wind and thermodynamic quantities relative to downdraft precipitation, are also revisited and compared to our findings over the Amazon. Downdrafts in MCSs and isolated cells are compared to inform decisions concerning their unified or separate treatment in next generation models. The effect of downdrafts on surface thermodynamics and boundary layer recovery are examined, and the origin height of the downdrafts explored, combining inferences from radar wind profiler data for vertical velocity and thermodynamic arguments from simple plume models. Lastly, statistics describing cold pool characteristics at the surface are presented and discussed for possible use as model diagnostics.

2 Data and Methods

Surface meteorological values (humidity, temperature, wind speed, precipitation) were obtained from the Aerosol Observing meteorological station (AOSMET) at the DOE ARM site in Manacapuru, Brazil, established as part of the GOAmazon campaign (site T3; ARM Climate Research Facility 2013a). The record used in this study spans 10 Jan 2014–20 Oct 2015. Values in this study are averaged at 30-min intervals. Equivalent potential temperature is computed following Bolton (1980). Sensible and latent heat fluxes (30-min) are derived from eddy

Atmos. Chem. Phys. Discuss., https://doi.org/10.5194/acp-2017-684
Manuscript under review for journal Atmos. Chem. Phys.
Discussion started: 28 August 2017

Atmospheric Chemistry and Physics
Discussions

correlation flux measurements obtained with the eddy covariance technique involving correlation of the vertical wind component with the horizontal winds, temperature, water vapor density, and carbon dioxide concentration (ARM Climate Research Facility 2014). A fast-response, three-dimensional sonic anemometer provides the wind components and speed of sound, while water vapor density is from an open-path infrared gas analyzer. Surface flux data from 03 Apr 2014–20 Oct 2015 are used here, with periods of missing and unreliable data excluded, as flagged by ARM.

Thermodynamic profiles are obtained from radiosonde measurements within 6 h of a convective event (ARM Climate Research Facility 2013b). Radiosondes are launched at approximately 01:30, 7:30, 13:30, and 19:30 LT each day, with occasional radiosondes at 10:30 LT in the wet season. Profiles of vertical velocity and radar reflectivity are obtained from a 1290 MHz radar wind profiler (RWP) reconfigured for precipitation modes. It has a beam width of 6^{o} (~ 1 km at 10 km AGL), a vertical resolution of 200 m, and a temporal resolution of 5 seconds (Giangrande et al. 2016).

Precipitation data at 25 km and 100 km, as well as convection classifications, are derived from an S-Band radar located approximately 67 km to the northeast of T3 at the Manaus Airport. Composite constant altitude low-level gridded reflectivity maps (constant altitude plan position indicators, CAPPIs) were generated, and the radar data were gridded to a Cartesian coordinate grid with horizontal and vertical resolution of 2 km and 0.5 km, respectively (ARM Climate Research Campaign Data, C. Schumacher, 2015). Rain rates were obtained from the 2.5 km reflectivity using the reflectivity-rain rate (Z-R) relation $Z=174.8R^{1.56}$ derived from disdrometer data (ARM Climate Research Campaign Data, C. Schumacher, 2015). The spatially averaged rainfall rate over a 25 km and 100 km grid box were used in this study. The center of the 100 km grid box is shifted slightly to the right of center with respect to the T3 site due to reduced data quality beyond a 110 km radius.

All convective events used in this study meet the following criteria: producing downdrafts that create a subsequent drop in θ_e at the surface of less than -5^{o} C in a 30-min period and having precipitation rates exceeding 10 mm h^{-1} in that same period. These criteria were chosen to examine the most intense downdraft events with the most well-defined vertical velocity signatures in the RWP data. Only data for events with complete vertical velocity data

Atmos. Chem. Phys. Discuss., https://doi.org/10.5194/acp-2017-684
Manuscript under review for journal Atmos. Chem. Phys.
Discussion started: 28 August 2017

Atmospheric Chemistry and Physics Discussions

coverage over the 1 h period spanning the passage of the convective cells and centered around the maximum precipitation were composited and evaluated.

Isolated convective cells were identified by S-Band composite reflectivity, as in Fig. 1, and are defined as being less than 50 km in any horizontal dimension (contiguous pixels with reflectivity > 30 dBZ) with a maximum composite reflectivity of greater than or equal to 45 dBZ. Following the criteria defined above, this resulted in the selection of 11 events, all of which were in the late morning or afternoon hours between 11:00 and 18:00 LT. Mesoscale convective systems follow the traditional definition of regions of contiguous precipitation at scales of 100 km or greater (contiguous pixels with reflectivity > 30 dBZ) in any horizontal dimension (e.g. Houze 1993; Houze 2004). All of the events sampled are characterized by a leading edge of convective cells with a trailing stratiform region (Fig. 1), which is the most common MCS type (Houze et al. 1990). The above criteria yielded 17 events: 11 in the late morning and early afternoon hours (11:00-18:00 LT) and 6 in the late evening/early morning hours (22:00-11:00 LT).

In Sect. 6, statistics are presented using nearly the entire two-year timeseries of meteorological variables at the GOAmazon site, as well as 15 years of data (1996–2010) from the DOE ARM site at Manus Island in the tropical western Pacific. One-hour averages are computed in $\Delta\theta_e$ and precipitation.

3 Surface Thermodynamics

Composites of surface meteorological variables are displayed in Fig. 2 for the 11 isolated cellular deep convective events coinciding with drops in equivalent potential temperature of -5^{o}C or less and precipitation rates greater than 10 mm h^{-1} (see Sect. 2). The composites are centered 3 h before and after the time marking the beginning of the sharpest decrease in surface θ_e. All differences quoted are the differences in values between the maximum and minimum values within the 1 h timeframe of convective cell passage, unless noted otherwise. All timeseries averaged in the composites are shifted to the mean value at 0.5 h, the timestep immediately following the minimum $\Delta\theta_e$, and error bars on the composites are +/- 1 standard deviation with respect to 0.5 h.

In the two hours leading the convection, the CWV increases by 4.3 mm. Values of θ_e are 353.6 K on average before passage of the cell. An hour after the passage, the θ_e value drops by an average 8.9° to an average value of 344.7 K. Since the isolated convective cells observed occur in the daytime hours, the relative humidity is seen to drop steadily throughout the 3 h period leading the convection following the rise in temperatures with the diurnal cycle. Once the cell passes, RH values rise to 81.6%, which indicates that the downdrafts are sub-saturated when they reach the surface. Temperatures drop by 4.4° C to 24.9° C, which is less of a drop in temperature than observed over mid-latitude sites (see Table 2 in Engerer et al. 2008 for a review of mid-latitude case studies) and specific humidity drops by 1.1 g kg^{-1} to 16.0 g kg^{-1}. Wind speeds reach 5.5 m s^{-1} on average, consistent with previous studies that document strong horizontal winds associated with the leading edges of cold pools (e.g. Fujita 1963; Wakimoto 1982), but are lower than the observed values for mid-latitude storms (Engerer et al. 2008). Additionally, surface pressure often increases with the existence of a cold pool and is referred to as the meso-high (Wakimoto 1982). Here, it increases marginally by 0.8 hPa, but this value is much less than the typical values observed in mid-latitudes (e.g. Goff 1976; Engerer et al. 2008). Lastly, 63% of the temperature and moisture depleted by the downdraft recovers within two hours of cell passage, with moisture recovering more quickly and by a greater percentage than temperature.

Complementary to those in Fig. 2, composites of surface meteorological variables are shown in Fig. 3 for the 17 MCSs with surface θ_e depressions of -5° C or less and coincident precipitation rates of 10 mm h^{-1} or greater. On average, the environment is more humid, as is seen in the CWV composite. Values of θ_e leading the passage of MCSs are a few degrees lower than the θ_e values leading the isolated cells. This is mostly due to lower surface temperatures. The precipitation occurs over a longer period than in the cases of isolated cells, as there is stratiform rain trailing the leading convective cells. The stratiform rain and associated downdrafts also sustain the cooling and drying of the near surface layers for many hours lagging the precipitation maximum. Column water vapor values leading the MCSs are slightly higher on average than observed leading the isolated cells, with an average maximum value of 59.8 mm. The relative humidity maximum in the cold pool is 90.2% (ΔRH = 14.2%), the specific humidity minimum is 15.5 g kg^{-1} (Δq = 1.7 g kg^{-1}), and the temperature minimum is 22.9° C (ΔT = 4.7° C), with winds gusting to an average of 6.3 m s^{-1} with the passage of the leading convective cells. The cold pools are thus cooler, drier, and nearer to saturation for the MCSs than for the isolated cells. It is worth noting that these statistics for MCSs are not greatly affected by the inclusion of nighttime events; composites for afternoon only MCSs yield similar results.

Overall, the environments in which MCSs live are moister, they have colder, drier cold pools that are nearer to saturation, the winds at their leading edges are gustier, and their boundary layers recover more slowly than for isolated cells.

4 Downdraft Origin and the Effects of Mixing

Many previous studies of moist convective processes use θ_e as a tracer since it is conserved in the condensation and evaporation of water and for dry and moist adiabatic processes (e.g., Emanuel 1994). Tracing surface θ_e to its equivalent value aloft has been used in many studies of tropical convection to examine potential downdraft origin heights (e.g. Zipser 1969; Betts 1973, 1976; Betts and Silva Dias 1979; Betts et al. 2002). This assumes that downdraft air conserves θ_e to a good approximation and that downdraft air originates at one height above ground level. Neither of these assumptions is likely to be true, as mixing is likely occurring between the descending air and the environmental air and thus originating from various levels. However, it can provide a useful reference point for further considerations.

We examine the mean θ_e profiles for MCSs and isolated cells, conditioned on the existence of a substantial drop in θ_e and precipitation rates above a threshold value, to place bounds on mixing and downdraft origin with simple plume computations. Matching the minimum θ_e value observed at the surface following the passage of convection to the minimum altitude at which those values are observed yields 1.3 km for isolated cells (left panel, Fig. 4) and 2.0 km for MCSs (right panel, Fig. 4). Again, this assumes that θ_e is conserved and that the air originates at one altitude. If instead we assume that substantial mixing occurs with the surrounding environment and that air originates at multiple levels in the lower troposphere, it would be plausible for more of the air reaching the surface to originate at altitudes greater than 1.3 and 2 km for isolated cells and MCSs, respectively. This has been alluded to in previous studies (e.g. Zipser, 1969; Gerken et al. 2016), which provide evidence that air originates in the middle troposphere.

To examine this, we mix air from above the altitude where the θ_e matched the surface value (shown in the composites in Figs. 2 and 3) downward towards the surface, varying the entrainment rate (constant with pressure). To start, we use a mixing of 0.001 hPa^{-1}, as this is the constant entrainment value used in Holloway and Neelin (2009) and Sahany et al. (2012), which produced realistic updraft buoyancy profiles over tropical oceans. For the MCS case, it is plausible that a downdraft could originate at a height of 2.3 km given this rate of mixing to reach the surface with characteristics given by Fig. 3. (Note that there is a spread in surface values and profile characteristics, but for simplicity we use mean values.) If instead the air were coming from the level of minimum θ_e, an assumption similar to that made by many downdraft parameterizations (e.g. Zhang and McFarlane 1995; Tiedke 1989; Kain and Fritsch 1990), mixing would need be 2.5 times greater. For the isolated cells, mixing rates appear to need to be much greater in order to produce results consistent with those seen at the surface. If we start out at 0.0025 hPa^{-1}, the rate sufficient for a minimum θ_e origin for the MCSs, this only yields an origin height of 1.5 km. If instead we assume the air originates near the level of minimum θ_e, mixing would need to be at least 0.006 hPa^{-1}. For reference, in the Tiedke and Zhang-McFarlane schemes, downdrafts mix with environmental air at a rate nearly double the rate of mixing in updrafts, which in the Tiedke scheme is 2 x 10^{-4} m^{-1}. This is similar to 0.0025 hPa^{-1} in pressure coordinates in the lower troposphere.

To summarize, this analysis is suggestive of bounds on mixing coefficients for downdraft parameterizations. Downdrafts would need to mix less substantially through the lower troposphere for MCSs than isolated cells to draw down air that matched the observed characteristics at the surface, and the rate of mixing needed to bring air down from the level of minimum θ_e would be 2.5 times greater for isolated cells than for the MCSs. In Sections 5 and 6, we provide a complementary probabilistic perspective on levels of origin.

5 Vertical Velocity and Downdraft Probability

Figure 5 composites reflectivity (Z), vertical velocity (w), and the probability of observing downdrafts ($w < 0$ m s^{-1}) for the 11 cases of isolated cellular convection meeting the minimum $\Delta\theta_e$ criteria of -5° C and minimum precipitation criteria of 10 mm h^{-1}. Time 0 is the time right before the sharpest decrease in θ_e, repeated from Fig. 2 in the top panel, and maximum precipitation. A 3 h window is composited for reference, but the interval of primary interest is the 1 h window within which the minimum $\Delta\theta_e$ and maximum precipitation are observed. To highlight the interval of interest, the 1 h intervals leading and lagging this period are masked out.

Atmos. Chem. Phys. Discuss., https://doi.org/10.5194/acp-2017-684
Manuscript under review for journal Atmos. Chem. Phys.
Discussion started: 28 August 2017

Atmospheric Chemistry and Physics Discussions

The drop in θ_e is coincident with the passage of the isolated cell and its main updraft and precipitation-driven downdraft. Mean reflectivity exceeding 40 dBZ is observed during this period, as are strong updrafts in the middle-upper troposphere. The cell then dissipates and/or moves past the site within an hour. A downdraft is observed directly below and slightly trailing the updraft core. This is the downdraft that is associated with the largest drop in surface θ_e. As is suggested in the literature, these are mainly driven by condensate loading and evaporation of precipitation and are negatively buoyant. The probability of observing negative vertical velocity (threshold < 0 m s^{-1}) within the 30 minutes of observed maxima in the absolute value of $\Delta\theta_e$ and precipitation is highest in the lower troposphere (0-2 km), consistent with precipitation-driven downdrafts observed in other studies (Sun et al. 1993; Cifelli and Rutledge 1994).

There is also a high probability of downdrafts in air near the freezing level (masked out in the vertical velocity retrievals, as there is large error associated with retrievals near the freezing level; Giangrande et al. 2016). It appears likely, however, that these downdrafts are discontinuous in height more often than not, as high probabilities are not observed coincidentally in the lowest levels beneath these downdrafts. These mid-upper level downdrafts are documented in previous studies of MCSs, suggesting that they form in response to the pressure field (e.g. Biggerstaff and Houze 1991), can occur quite close to the updraft (Lily 1960; Fritsch 1975), and are positively buoyant (Fovell and Ogura 1988; Jorgensen and LeMone 1989; Sun et al. 1993). These motions produce gravity waves in upper levels, as is discussed in Fovell et al. (1992).

Figure 6 shows the same composites for the 17 MCSs observed. They, too, have high reflectivity (mean > 40 dBZ) in the 30 minutes coincident with the minimum θ_e and a defined updraft extending up to the upper troposphere. Downdrafts occurring coincident with the minimum θ_e are observed directly below the updraft signature in the mean vertical velocity panel, and the probabilities are greatest below the freezing level. There is also evidence of mesoscale downdrafts in the trailing stratiform region of the MCSs, which Miller and Betts (1977) suggest are more dynamically driven than the precipitation-driven downdrafts associated with the leading-edge convection. These sustain the low θ_e air in the boundary layer for hours after the initial drop, observed in Fig. 3. Vertical motions in the stratiform region are weaker than in the convective region, and on average, as in Cifelli and Rutledge (1994), rarely exceed 1 m s^{-1}.

Figure 7 is a concise summary of the results presented in Figs. 5 and 6, showing the mean vertical velocity within the 30-min of sharpest $\Delta\theta_e$ for MCSs and isolated cells. Previous studies using radar wind profilers have shown mean updraft and downdraft strength increases with height (May and Rajopadhyaya 1999; Kumar et al. 2015; Giangrande et al. 2016), consistent with our results here for both isolated and organized deep convection. The corresponding mean probability is shown in the right panel. The probability of downdrafts for both isolated cells and MCSs increases nearly linearly towards the surface below the freezing level. Thus, the behavior in the lowest 3 km summarizes our results from the previous two figures and suggests that downdrafts accumulate air along their descent, analogous to mixing. Probabilities, which can be interpreted loosely as convective area fractions (Kumar et al. 2015; Giangrande et al. 2016), are also largest below the freezing level for downdrafts and in the 3-7 km region for updrafts. The probability and vertical velocity for both MCSs and isolated cells correspond to mass flux profiles that increase nearly linearly throughout the lower troposphere for updrafts and that decrease nearly linearly throughout the lower troposphere for downdrafts, as seen in Giangrande et al. (2016) over a broader range of convective conditions.

These results suggest that in most downdrafts, a substantial fraction of the air reaching the surface originates in the lowest 3 km within both organized and unorganized convective systems. Several observational studies corroborate the evidence presented here that a majority of the air reaching the surface in deep convective downdrafts originates at low-levels (Betts 1976; Barnes and Garstang 1982; Betts et al. 2002). Betts 1976 concluded that the downdraft air descends approximately only the depth of the subcloud layer (~150 mb). Betts et al. (2002) cited a range of 765-864 hPa for the first levels at which the surface θ_e values matched those of the air aloft. Additionally, there are many modeling studies that provide evidence of these low-level origins (Moncrieff and Miller, 1976; Torri and Kuang, 2016). Recently, Torri and Kuang (2016) used a Lagrangian particle dispersion model to show that precipitation-driven downdrafts originate at very low levels, citing an altitude of 1.5 km from the surface. These conclusions are consistent with our results here, suggesting that downdraft parameterizations substantially weight the contribution of air from the lower troposphere (e.g. with substantial mixing, modifying height of downdraft origin).

6 Relating Cold Pool Thermodynamics to Precipitation

As seen in previous sections, the passage of both organized and unorganized convective cells can lead to substantial decreases in θ_e resulting mainly from precipitation-driven downdrafts formed from the leading convective cells. In this section, we search for robust statistical relationships between key thermodynamic variables for potential use in improving downdraft parameterizations in GCMs. These statistics differ from those presented in Figs. 2-7, as these statistics are not conditioned on convection type and sample both precipitating and non-precipitating points within the timeseries analyzed. All data available at the surface meteorological station during the GOAmazon campaign from 10 Jan 2014–20 Oct 2015 are included in these statistics.

The first of these statistics conditionally averages precipitation rate by $\Delta\theta_e$ (Fig. 8), variants of which have been discussed in previous studies (Barnes and Garstang 1982; Wang et al. 2016). Our statistics mimic those shown in previous work relating column-integrated moisture to deep convection over tropical land (Schiro et al. 2016) and ocean (Neelin et al. 2009; Holloway and Neelin 2009). The direction of causality in the CWV-precipitation statistics, however, is the opposite of what is presented here. CWV is thought to primarily be the cause of intense precipitation and deep convection, while here the $\Delta\theta_e$ observed is a direct result of the precipitation processes and associated downdraft. Nevertheless, examining the distribution of $\Delta\theta_e$ observed at the surface and magnitudes of the rain rates associated with the highest drops in $\Delta\theta_e$ across different regions in the tropics can place bounds on downdraft behavior. We will also conditionally average $\Delta\theta_e$ by precipitation rate, a more physically consistent direction of causality.

Figure 8 shows precipitation rate binned by $\Delta\theta_e$ for in-situ precipitation and radar precipitation. Bins are 1° C in width and precipitating events are defined as having rain rates greater than 1 mm h^{-1}. These statistics mainly suggest that any substantial decrease in θ_e at the surface occurs coincidently with heavy precipitation, which is particularly evident from the sharp increase in probability of precipitation (middle panel). The width of the distribution of precipitating points is of greatest interest here. The distribution of precipitating points peaks just shy of a $\Delta\theta_e$ of 0° C, indicating that most precipitation events have low rain rates and do not occur coincidently with an appreciable drop in $\Delta\theta_e$. The frequency of precipitation drops off roughly exponentially towards lower $\Delta\theta_e$. An interesting feature is the lower bound observed in the $\Delta\theta_e$ near -15° C. Examining mean profiles in Fig. 5 show that, on average, this value of -15° C would be consistent with air originating from the level of minimum θ_e and descending undiluted to the surface. The frequency of observing these values suggests that air very rarely

Atmos. Chem. Phys. Discuss., https://doi.org/10.5194/acp-2017-684
Manuscript under review for journal Atmos. Chem. Phys.
Discussion started: 28 August 2017

Atmospheric Chemistry and Physics
Discussions

reaches the surface from these altitudes (3 km or higher) undiluted. The θ_e probability distribution is consistent with the results of Sect. 5, indicating that the probability of air from a given level of origin reaching the surface increases toward the surface through the lowest 3 km.

S-Band radar data are averaged in 25 km and 100 km grid boxes surrounding the GOAmazon site to examine the precipitation-$\Delta\theta_e$ relation with model diagnostics in mind (Fig. 8). Out to 25 km, the statistics are very similar to those observed using in situ precipitation. Theoretical (Romps and Jevanjee 2015), modeling (Tompkins 2001; Feng et al. 2015), and observational (Feng et al. 2015) studies have all examined typical sizes of cold pools, which are on the order of 25 km in diameter for any one cell. Cold pools can combine, however, to form a larger, coherent mesoscale-sized cold pool (radius of 50 km or greater), as is commonly associated with mesoscale convective systems (Fujita 1959; Johnson and Hamilton 1988). Therefore, it is likely that our use of the in situ $\Delta\theta_e$, assuming cold pool properties are somewhat homogeneous in space, is appropriate for scales up to 25 km. Beyond this scale, it is likely that the $\Delta\theta_e$ would be smoothed by averaging, particularly for the smaller isolated cells, as would precipitation. For 100 km, the precipitation is smoothed by averaging, which would likely degrade further if information of 100 km mean surface thermodynamics were available. This suggests that comparing these statistics to those produced with model output for diagnostic purposes would yield a narrower range of $\Delta\theta_e$ and lower conditionally averaged rain rates.

Figure 9 shows remarkable similarity in these statistics when comparing across regions to a DOE ARM site at Manus Island in the tropical western Pacific. As $\Delta\theta_e$ decreases, in situ precipitation rates sharply increase. The distributions, as well as the steepness and locations of the pickups, are remarkably consistent. Again, the sharpness of these curves is a result of the strongest precipitation events coinciding with the strongest decreases in θ_e, shown in the middle panels in Fig. 9, where the probability of observing precipitation is greatest at lower $\Delta\theta_e$.

It is then of interest to see if for a given precipitation rate we can expect a particular $\Delta\theta_e$, as this is the proper direction of causality. Figure 10 conditionally averages $\Delta\theta_e$ by precipitation rate (1-h averages). The maximum $\Delta\theta_e$ within a 3-h window of a given precipitation rate is averaged to minimize the effects of local precipitation maxima occurring slightly before or after the minimum in $\Delta\theta_e$. Comparing Fig. 9 and Fig. 10 shows that there can be strong precipitation events without large, corresponding decreases in surface θ_e, but that large decreases in surface θ_e are almost always associated with heavy precipitation.

Beyond about 10 mm h^{-1} there is high probability of observing large, negative $\Delta\theta_e$ and an apparent limit in mean θ_e decreases with rain rate. This makes physical sense, as discussed above (see also Barnes and Garstang 1982), since cooling is limited by the maximum difference between the surface θ_e and the θ_e minimum aloft. The average $\Delta\theta_e$ for rain rates exceeding 10 mm h^{-1} is about -5^{o} C for the Amazon and -4^{o} C for Manus Island. This statistic could be of use in constraining downdraft parameters to be consistent with surface cooling and drying observed in nature. There are still, however, open questions about scale dependence and how much cooling or drying should be observed for varying space and time scales. This result is likely applicable to GCM grid scales of 0.25^{o} or less, as is suggested from the results in Fig. 9, but would be of lesser magnitude at scales more comparable to typical GCM grids (100 km or greater). Overall, if convective precipitation is present in a GCM grid, a corresponding $\Delta\theta_e$ should result within a range consistent to those observed here, subject to scale dependence.

7 Conclusions

Convective events sampled during the GOAmazon campaign compare downdraft characteristics between MCSs and isolated cells and examine their respective effects on surface thermodynamics. All events included in the analysis passed directly over the GOAmazon site with minimum precipitation rates of 10 mm h^{-1} and $\Delta\theta_e$ less than or equal to -5^{o} C. The isolated events sampled occurred in the afternoon hours only and were characterized by average decreases of 1.1 g kg^{-1} in specific humidity, 3.9^{o} C in temperature, and 8.0^{o} C in θ_e, with an increase of 5.5 m s^{-1} in wind speed at the surface. More than half of the deficit in θ_e observed with the passage of the cells recovers within 2 h, on average, with the moisture recovering faster than temperature and a larger fraction of the total θ_e recovered. MCSs show similar decreases in temperature (3.7^{o} C) but larger decreases in moisture (1.5 g kg^{-1}) and thus θ_e (9.1^{o} C) at the surface. The θ_e recovers more slowly for MCSs due to the mesoscale downdrafts and associated precipitation in their trailing stratiform regions.

Vertical velocity profiles from a radar wind profiler show that the probability of observing downdraft air during the 30 minutes of observed minimum $\Delta\theta_e$ increases with decreasing height in the lowest 3 km for both isolated cells and MCSs. This vertical structure of the downdraft probability is consistent with negative vertical velocities originating at various levels within this layer and continuing to the surface. Considering complementary thermodynamic arguments, without mixing, profiles of θ_e suggest that origin levels at average altitudes of 1.3 and 2 km for isolated cells and MCSs, respectively, would be consistent with average cold pool θ_e for these cases. A minimum in θ_e is observed between 3 and 7 km, on average, so for air to originate above 3 km, simple plume calculations suggest that downdrafts in MCSs would have to be mixing with environmental air at an approximate rate of 0.0025 hPa^{-1} along descent and at a rate roughly 2.5 times greater (0.006 hPa^{-1}) for isolated cells. This would imply mass entering the downdraft throughout the lowest few kilometers. Overall the vertical velocity and thermodynamic constraints are consistent in suggesting a spectrum of downdraft mass origin levels throughout the lowest few kilometers.

Robust statistical relationships between $\Delta\theta_e$ and precipitation are examined from nearly two years of data at the GOAmazon site and 15 years of data at the DOE ARM site at Manus Island in the tropical western Pacific. We conditionally average precipitation by $\Delta\theta_e$, similar to the statistics of precipitation conditioned on a thermodynamic quantity we consider for convective onset statistics. Here, however, the most likely direction of causality differs in that the θ_e drop is caused by the downdraft that delivers the precipitation (as opposed to the thermodynamic profile providing convective available potential energy for an updraft). For in situ precipitation, the conditional average precipitation exhibits a sharp increase with decreasing $\Delta\theta_e$, which is similar in magnitude over land and ocean, reaching roughly 10 mm $hour^{-1}$ at a $\Delta\theta_e$ of -10° C. For area-averaged precipitation on scales typical of GCM grids, precipitation magnitude is lower for strong, negative $\Delta\theta_e$, consistent with the points with large $\Delta\theta_e$ occurring at localized downdraft locations within a larger system with smaller area-average precipitation. The probability distributions of $\Delta\theta_e$ (for precipitating and non-precipitating points) over land and ocean are also remarkably similar. Distributions show exponentially decreasing probability with decreasing $\Delta\theta_e$, providing additional evidence that downdraft plumes originating in the lowest levels are orders of magnitude more likely than plumes descending with little mixing from the height of minimum θ_e. Conditionally averaging $\Delta\theta_e$ by precipitation (the most likely direction of causality) suggests an average limit in $\Delta\theta_e$ of -4° C to -5° C given high precipitation typical of downdraft conditions. The corresponding 90th percentile yields $\Delta\theta_e$ of roughly -10° C, consistent with results obtained from composting strong downdrafts. The robustness of these statistics over land and ocean, and to averaging in space at scales appropriate to a typical GCM resolution, suggests possible use of these statistics as model diagnostic tools and observational constraints for downdraft parameterizations.

Acknowledgments

The U.S. Department of Energy Atmospheric Radiation Measurement (ARM) Climate Research Facility GOAmazon and Tropical West Pacific field campaign data were essential to this work. This research was supported in part by the Office of Biological and Environmental Research of the U.S. Department of Energy Grant DE-SC0011074, National Science Foundation Grant AGS-1505198, National Oceanic and Atmospheric Administration Grant NA14OAR4310274, and a Dissertation Year from the University of California, Los Angeles Fellowship (KS). Parts of this material have been presented at the Fall 2016 meeting of the American Geophysical Union and have formed part of K. Schiro's PhD thesis. We thank S. Giangrande for providing pre-processed radar wind profiler data and for helpful discussions.

Atmos. Chem. Phys. Discuss., https://doi.org/10.5194/acp-2017-684
Manuscript under review for journal Atmos. Chem. Phys.
Discussion started: 28 August 2017

References

Atmospheric Radiation Measurement (ARM) Climate Research Facility. 2013(a), updated hourly. Meteorological Measurements associated with the Aerosol Observing System (AOSMET). 2014-01-10 to 2015-10-20, ARM Mobile Facility (MAO) Manacapuru, Amazonas, Brazil; MAOS (S1). Compiled by A. Koontz, J. Kyrouac and S. Springston. Atmospheric Radiation Measurement (ARM) Climate Research Facility Data Archive: Oak Ridge, Tennessee, USA. Data set accessed at http://dx.doi.org/10.5439/1025153.

Atmospheric Radiation Measurement (ARM) Climate Research Facility. 2013(b), updated hourly. Balloon-Borne Sounding System (SONDEWNPN). 2014-01-10 to 2015-10-20, ARM Mobile Facility (MAO) Manacapuru, Amazonas, Brazil; AMF1 (M1). Compiled by D. Holdridge, J. Kyrouac and R. Coulter. Atmospheric Radiation Measurement (ARM) Climate Research Facility Data Archive: Oak Ridge, Tennessee, USA. Data set accessed at http://dx.doi.org/10.5439/1021460.

Atmospheric Radiation Measurement (ARM) Climate Research Facility. 2014, updated hourly. Eddy Correlation Flux Measurement System (30ECOR). 2014-04-03 to 2015-10-20, ARM Mobile Facility (MAO) Manacapuru, Amazonas, Brazil; AMF1 (M1). Compiled by D. Cook. Atmospheric Radiation Measurement (ARM) Climate Research Facility Data Archive: Oak Ridge, Tennessee, USA. Data set accessed at http://dx.doi.org/10.5439/1025039.

Atmospheric Radiation Measurement (ARM) Climate Research Campaign Data, Observations and Modeling of the Green Ocean Amazon (GOAMAZON), 2015. SIPAM Manaus S-Band Radar. 10 Jan 2014–20 Oct 2015, 36° 3.1489° S, 59.9914° W, Manaus, Amazonas, Brazil (T1). Processed by C. Schumacher. Data set accessed Feb 2017 at iop.archive.arm.gov.

Barnes, G. M. and M. Garstang, 1982: Subcloud Layer Energetics of Precipitating Convection. *Monthly Weather Review*, **110**, 102-117.

Betts, A., 1973: Non-precipitating cumulus convection and its parameterization. *Quarterly Journal of the Royal Meteorological Society*, **99**, 178-196.

Betts, A. K., 1976: The thermodynamic transformation of the tropical subcloud layer by precipitation and downdrafts. *Journal of the Atmospheric Sciences*, **33**, 1008-1020.

Atmos. Chem. Phys. Discuss., https://doi.org/10.5194/acp-2017-684
Manuscript under review for journal Atmos. Chem. Phys.
Discussion started: 28 August 2017

Atmospheric Chemistry and Physics
Open Access
Discussions

Betts, A. K., and M. F. Silva Dias, 1979: Unsaturated downdraft thermodynamics in cumulonimbus. *Journal of the Atmospheric Sciences*, **36**(6), 1061-1071.

Betts, A. K., and C. Jakob, 2002: Study of diurnal cycle of convective precipitation over Amazonia using a single column model, *Journal of Geophysical Research.,* **107**, 4732.

Biggerstaff, M. I., and R. A. Houze Jr, 1991: Kinematic and precipitation structure of the 10–11 June 1985 squall line. *Monthly Weather Review*, **119**, 3034-3065.

Boing, S. J., H J. J. Jonker, A. P. Siebesma, and W. W. Grabowski, 2012: Influence of the Subcloud Layer on the Development of a Deep Convective Ensemble. *Journal of the Atmospheric Sciences,* **69**, 2682-2698.

Bolton, D., 1980: The computation of equivalent potential temperature. *Monthly Weather Review*, **108**, 1046-1053.

Byers, H. R. and R. R. Braham, 1949: The thunderstorm: report of the Thunderstorm Project. *US Government Printing Office.*

Cifelli, R., and S. A. Rutledge, 1994: Vertical motion structure in maritime continent mesoscale convective systems: Results from a 50-MHz profiler. *Journal of the Atmospheric Sciences*, **51**, 2631-2652.

Del Genio, A. D., Y. Chen, D. Kim, M.-S. Yao, 2012: The MJO Transition from Shallow to Deep Convection in CloudSat/CALIPSO Data and GISS GCM Simulations. *Journal of Climate,* **25**, 3755-3770.

Emanuel, K. A., 1994: Atmospheric Convection. 1st ed. Oxford University Press, 580 pp.

Engerer, N. A., D. J. Stensrud, and M. C. Coniglio, 2008: Surface characteristics of observed cold pools. *Monthly Weather Review*, **136**, 4839-4849.

Feng, Z., S. Hagos, A. K. Rowe, C. D. Burleyson, M. N. Martini, and S. P. Szoeke, 2015: Mechanisms of convective cloud organization by cold pools over tropical warm ocean during the AMIE/DYNAMO field campaign. *Journal of Advances in Modeling Earth Systems*, **7**, 357-381.

Fritsch, 1975: Cumulus dynamics: Local compensating subsidence and its implications for cumulus parameterization. *Pure and Applied Geophysics,* **113***,* 851-867.

Fovell, R. G. and Ogura, Y., 1988: Numerical simulation of a midlatitude squall line in two dimensions. *Journal of the Atmospheric Sciences*, **45**, 3846-3879.

Atmos. Chem. Phys. Discuss., https://doi.org/10.5194/acp-2017-684
Manuscript under review for journal Atmos. Chem. Phys.
Discussion started: 28 August 2017

Fovell, R., D. Durran, and J. R. Holton, 1992: Numerical simulations of convectively generated stratospheric gravity waves. *Journal of the Atmospheric Sciences*, **49**, 1427-1442.

Fovell, R. G. and P. H. Tan, 1998: The temporal behavior of numerically simulated multicell-type storms. Part II: The convective cell life cycle and cell regeneration. *Monthly Weather Review*, **126**, 551-577.

Fujita, T., 1959: Precipitation and cold air production in mesoscale thunderstorm systems. *Journal of Meteorology*, **16**, 454-466.

Gerken, T., D. Wei, R. J. Chase, J. D. Fuentes, C. Schumacher, L. Machado, R. V. Andreoli et al., 2016: Downward transport of ozone rich air and implications for atmospheric chemistry in the Amazon rainforest. *Atmospheric Environment,* **124**, 64-76.

Giangrande, S. E., T. Toto, M. P. Jensen, M. J. Bartholomew, Z. Feng, A. Protat, C. R. Williams, C. Schumacher, and L. Machado, 2016: Convective cloud vertical velocity and mass-flux characteristics from radar wind profiler observations during GoAmazon2014/5. *Journal of Geophysical Research: Atmospheres*, **121**(21).

Goff, R., 1976: Vertical structure of thunderstorm outflows. *Monthly Weather Review*, **104**, 1429-1440.

Hohenegger, C. and C. S. Bretherton, 2011: Simulating deep convection with a shallow convection scheme. *Atmospheric Chemistry and Physics*, **11**(20), 10389-10406.

Holloway, C. E., and J. D. Neelin, 2009: Moisture Vertical Structure, Column Water Vapor, and Tropical Deep Convection. *Journal of the Atmospheric Sciences,* **66**, 1665–1683.

Houze, R. A., B. F. Smull, and P. Dodge, 1990: Mesoscale organization of springtime rainstorms in Oklahoma. *Monthly Weather Review*, **118**, 613-654.

Houze, R.A., 1993: *Cloud Dynamics*, 573 pp., Academic, San Diego, Calif.

Houze, R. A., 2004: Mesoscale convective systems. *Reviews of Geophysics*, **42**(4).

Johnson, R. H., and P. J. Hamilton, 1988: The relationship of surface pressure features to the precipitation and airflow structure of an intense midlatitude squall line. *Monthly Weather Review*, **116**, 1444-1473.

Jorgensen, D. P. and M. A. LeMone, 1989: Vertical velocity characteristics of oceanic convection. *Journal of the Atmospheric Sciences*, **46**, 621-640.

Kamburova, P. L. and F. H. Ludlam, 1966: Rainfall evaporation in thunderstorm downdraughts. *Quarterly Journal of the Royal Meteorological Society*, **92**, 510-518.

Kain, J. S., and J. M. Fritsch, 1990: A one-dimensional entraining/detraining plume model and its application in convective parameterization. *Journal of the Atmospheric Sciences*, **47**, 2784-2802.

Khairoutdinov, M., and D. Randall, 2006: High-resolution simulation of shallow-to-deep convection transition over land, *Journal of the Atmospheric Sciences,* **63**, 3421 – 3436.

Khairoutdinov, M. F., S. K. Krueger, C. H. Moeng, P. A. Bogenschutz and D. A. Randall, 2009: Large-eddy simulation of maritime deep tropical convection. *Journal of Advances in Modeling Earth Systems*, **1**(4).

Knupp, K. R. and W. R. Cotton, 1985: Convective cloud downdraft structure: An interpretive survey. *Reviews of Geophysics*, **23**, 183-215.

Kumar, V. V., C. Jakob, A. Protat, C. R. Williams, and P. T. May, 2015: Mass-flux characteristics of tropical cumulus clouds from wind profiler observations at Darwin, Australia. *Journal of the Atmospheric Sciences*, **72**, 1837–1855.

Langenbrunner, B. and J. D. Neelin: Multiobjective constraints for climate model parameter choices: Pragmatic Pareto fronts in CESM1. *Journal of Advances in Modeling Earth Systems*, accepted.

Li, Z., P. Zuidema, and P. Zhu, 2014: Simulated convective invigoration processes at trade wind cumulus cold pool boundaries. *Journal of the Atmospheric Sciences*, **71**, 2823-2841.

Lily, D., 1960: On the theory of disturbances in a conditionally unstable atmosphere. *Monthly Weather Review,* **88**, 1-17.

Lima, M. A., and J. W. Wilson, 2008: Convective storm initiation in a moist tropical environment. *Monthly Weather Review*, **136**, 1847-1864.

Martin, S. T., P. Artaxo, L. A. T. Machado, A. O. Manzi, R. A. F. Souza, C. Schumacher, J. Wang, M. O. Andreae, H. M. J. Barbosa, J. Fan, G. Fisch, A. H. Goldstein, A. Guenther, J. L. Jimenez, U. Pöschl, M. A. Silva Dias, J. N. Smith, and M. Wendisch, 2016: Introduction: Observations and Modeling of the Green Ocean Amazon (GoAmazon2014/5). *Atmospheric Chemistry and Physics,* **16**, 4785-4797.

Maloney, E. D. and D. L. Hartmann, 2001: The sensitivity of intraseasonal variability in the NCAR CCM3 to changes in convective parameterization. *Journal of Climate*, **14**, 2015-2034.

Atmos. Chem. Phys. Discuss., https://doi.org/10.5194/acp-2017-684
Manuscript under review for journal Atmos. Chem. Phys.
Discussion started: 28 August 2017

May, P. T. and D. K. Rajopadhyaya, 1998: Vertical Velocity Characteristics of Deep Convection over Darwin, Australia. *Monthly Weather Review*, **127**, 1056-1071.

Miller, M. J., and A. K. Betts, 1977: Traveling convective storms over Venezuela. *Monthly Weather Review,* **105**, 833-848.

Moncrieff, M. W. and M. J. Miller, 1976: The dynamics and simulation of tropical cumulonimbus and squall lines. *Quarterly Journal of the Royal Meteorological Society*, **102**, 373-394.

Neelin, J.D., O. Peters, and K. Hales, 2009: The Transition to Strong Convection. *Journal of the Atmospheric Sciences,* **66**, 2367–2384.

Pritchard, M. S., M. W. Moncrieff, and R. C. Somerville, 2011: Orogenic propagating precipitation systems over the United States in a global climate model with embedded explicit convection. *Journal of the Atmospheric Sciences*, **68**, 1821-1840.

Purdom, J. F., 1976: Some uses of high-resolution GOES imagery in the mesoscale forecasting of convection and its behavior. *Monthly Weather Review*, **104**, 1474-1483.

Rotunno, R., J. B. Klemp, and M. L. Weisman, 1988: A Theory for Strong, Long-Lived Squall Lines. *Journal of the Atmospheric Sciences,* **45**, 463–485.

Rio, C., F. Hourdin, J. Y. Grandpeix, and J. P. Lafore, 2009: Shifting the diurnal cycle of parameterized deep convection over land. *Geophysical Research Letters*, **36**.

Romps, D. M., and N. Jeevanjee, 2016: On the sizes and lifetimes of cold pools. *Quarterly Journal of the Royal Meteorological Society*, **142**, 1517-1527.

Rowe, A. K., and R. A. Houze, Jr., 2015: Cloud organization and growth during the transition from suppressed to active MJO conditions. *Journal of Geophysical Research: Atmospheres.*, **120**, 10324–10350.

Sahany, S. and R. S. Nanjundiah, 2008: Impact of convective downdrafts on model simulations: results from aqua-planet integrations. In *Annales geophysicae: atmospheres, hydrospheres and space sciences* (Vol. 26, No. 7, p. 1877).

Sahany, S., J. D. Neelin, K. Hales, and R. B. Neale, 2012: Temperature-moisture dependence of the deep convective transition as a constraint on entrainment in climate models. *Journal of the Atmospheric Sciences,* **69**, 1340–1358.

Schiro, K. A., J. D. Neelin, D. K. Adams, and B. R. Lintner, 2016: Deep Convection and Column Water Vapor over Tropical Land versus Tropical Ocean: A Comparison between the

Atmos. Chem. Phys. Discuss., https://doi.org/10.5194/acp-2017-684
Manuscript under review for journal Atmos. Chem. Phys.
Discussion started: 28 August 2017

Atmospheric Chemistry and Physics
Open Access
Discussions

Amazon and the Tropical Western Pacific. *Journal of the Atmospheric Sciences*, **73**, 4043-4063.

Schlemmer, L., and C. Hohenegger, 2014: The Formation of Wider and Deeper Clouds as a Result of Cold-Pool Dynamics. *Journal of the Atmospheric Sciences,* **71**, 2842–2858.

Srivastava, R. C., 1987: A model of intense downdrafts driven by the melting and evaporation of precipitation. *Journal of the Atmospheric Sciences*, **44**, 1752-1774.

Sun, J., S. Braun, M. I. Biggerstaff, R. G. Fovell, and R. A. Houze Jr, 1993: Warm upper-level downdrafts associated with a squall line. *Monthly Weather Review*, **121**(10), 2919-2927.

Terai, C. R. and R. Wood, 2013: Aircraft observations of cold pools under marine stratocumulus. *Atmospheric Chemistry and Physics*, **13**(19), 9899-9914.

Tiedtke, M., 1989: A comprehensive mass flux scheme for cumulus parameterization in large-scale models. *Monthly Weather Review*, **117**(8), 1779-1800.

Tompkins, A. M., 2001: Organization of tropical convection in low vertical wind shears: The role of cold pools. *Journal of the Atmospheric Sciences,* **58**, 1650–1672

Torri, G. and Z. Kuang, 2016: A Lagrangian study of precipitation-driven downdrafts. *Journal of the Atmospheric Sciences*, **73**(2), 839-854.

Wakimoto, R. M., 1982: The life cycle of thunderstorm gust fronts as viewed with Doppler radar and rawinsonde data. *Monthly Weather Review*, **110**(8), 1060-1082.

Wang, H. and G. Feingold, 2009: Modeling mesoscale cellular structures and drizzle in marine stratocumulus. Part I: Impact of drizzle on the formation and evolution of open cells. *Journal of the Atmospheric Sciences*, **66**, 3237-3256.

Wang, J., R. Krejci, S. Giangrande, C. Kuang, H.M. Barbosa, J. Brito, S. Carbone, X. Chi, J. Comstock, F. Ditas, and J. Lavric, 2016: Amazon boundary layer aerosol concentration sustained by vertical transport during rainfall. *Nature,* **539**, 416-419.

Weisman, M. L., and J. B. Klemp, 1986: Characteristics of isolated convective storms. In *Mesoscale Meteorology and Forecasting* (pp. 331-358). American Meteorological Society.

Wilson, J. W., and W. E. Schreiber, 1986: Initiation of convective storms at radar-observed boundary-layer convergence lines. *Monthly Weather Review*, **114**(12), 2516-2536.

Zhang, G. J., and N. A. McFarlane, 1995: Sensitivity of climate simulations to the parameterization of cumulus convection in the Canadian Climate Centre general circulation model. *Atmosphere-ocean,* **33**, 407-446.

Zipser, E. J., 1969: The role of organized unsaturated convective downdrafts in the structure and rapid decay of an equatorial disturbance. *Journal of Applied Meteorology*, **8**, 799-814.

Zipser, E. J., 1977: Mesoscale and convective–scale downdrafts as distinct components of squall-line structure. *Monthly Weather Review*, **105**, 1568-1589.

Zuidema, P., Z. Li, R. J. Hill, L. Bariteau, B. Rilling, C. Fairall, W. A. Brewer, B. Albrecht, and J. Hare, 2012: On trade wind cumulus cold pools. *Journal of the Atmospheric Sciences*, **69**, 258-280.

Atmos. Chem. Phys. Discuss., https://doi.org/10.5194/acp-2017-684
Manuscript under review for journal Atmos. Chem. Phys.
Discussion started: 28 August 2017

Atmospheric Chemistry and Physics
Open Access
Discussions

Figures

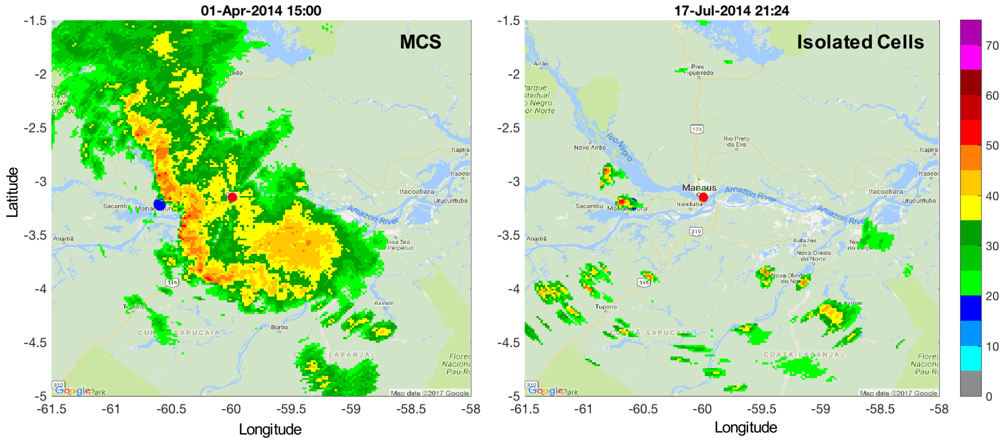

Figure 1: Examples from S-Band Radar on 01 Apr 2014 at 15:00 UTC (11:00 LT) before the passage of an MCS, and at 17 Jul 2017 at 21:24 UTC (17:24 LT) after the passage of an isolated cell. The red dot indicates the location of the S-Band radar, and the blue dot indicates the location of the main GOAmazon site (T3).

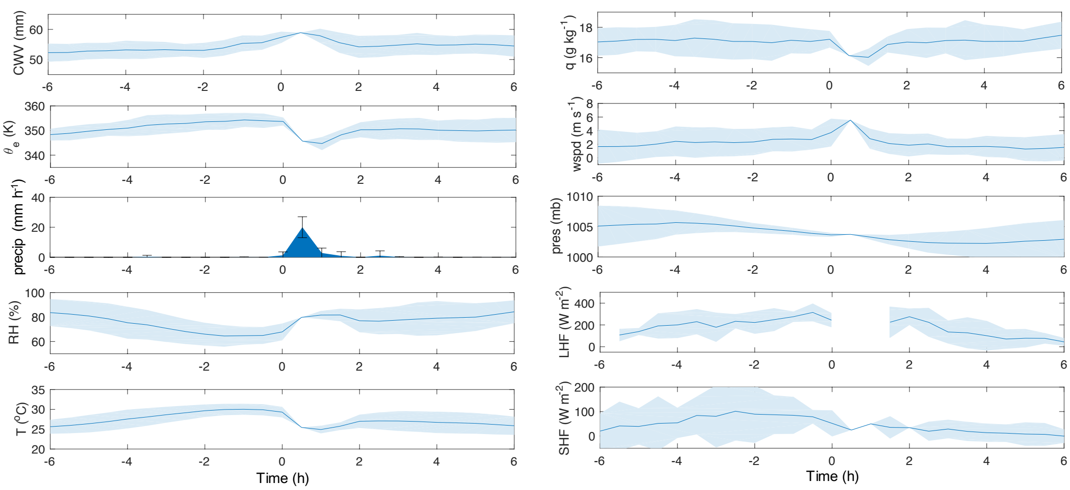

Figure 2: Composites of meteorological variables from the AOSMET station at site T3 6 h leading and 6 h lagging the 30-minute interval right before the drop in equivalent potential temperature (2nd panel) and precipitation maximum (3rd panel) coincident with the passage of isolated cells. Error bars are +/- 1 standard deviation with respect to 0.5 h.

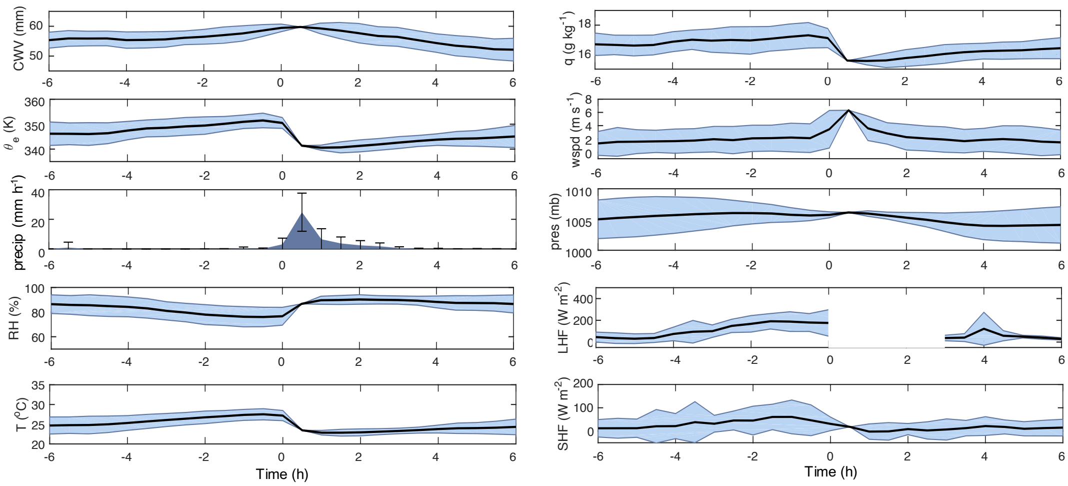

Figure 3: Same as Fig. 2, except for MCSs.

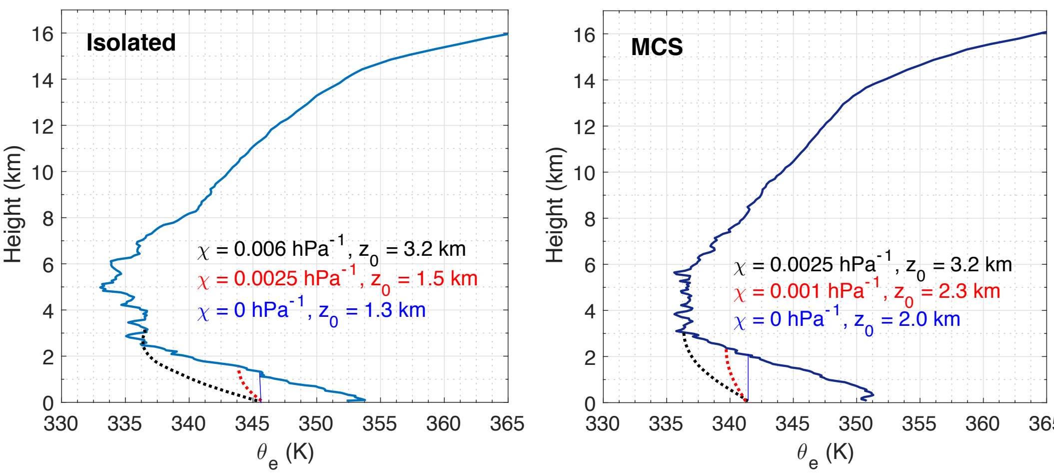

Figure 4: Mean profiles of θ_e for isolated cells (left) and MCSs (right) within 6 h leading the passage of a deep convective event. Dashed lines indicate the mean descent path for plumes originating at various altitudes and mixing with the environment at various rates; solid blue line shows mean descent without mixing.

Atmos. Chem. Phys. Discuss., https://doi.org/10.5194/acp-2017-684
Manuscript under review for journal Atmos. Chem. Phys.
Discussion started: 28 August 2017

Atmospheric Chemistry and Physics
Open Access
Discussions

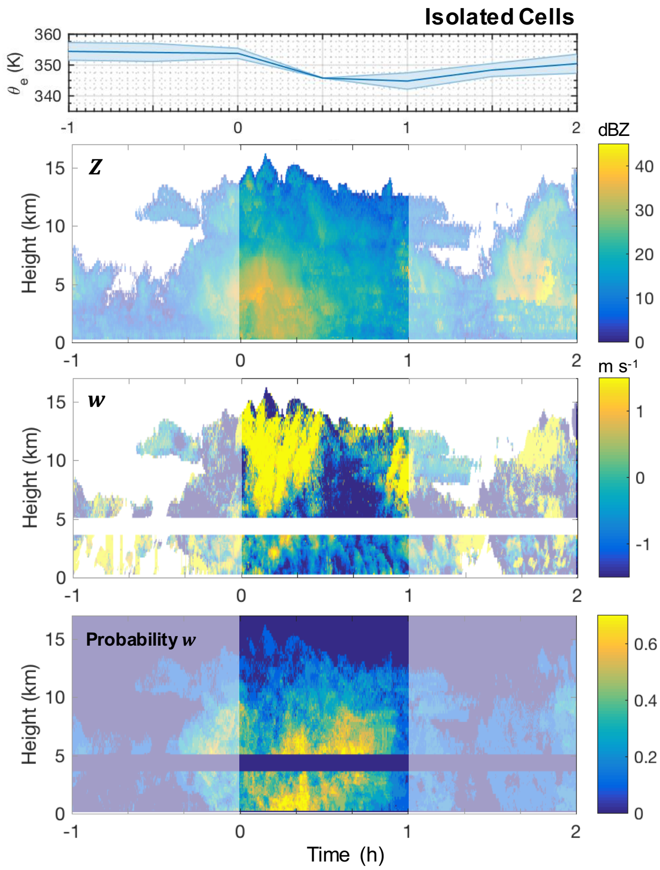

Figure 5: The composite θ_e surrounding minimum $\Delta\theta_e$, as in Fig. 2 (top panel), mean reflectivity (dBZ; second panel), mean vertical velocity (third panel; m s^{-1}), and probability of w < 0 m s^{-1} (bottom panel) measured by the radar wind profiler at T3 leading and lagging the passage of isolated cells.

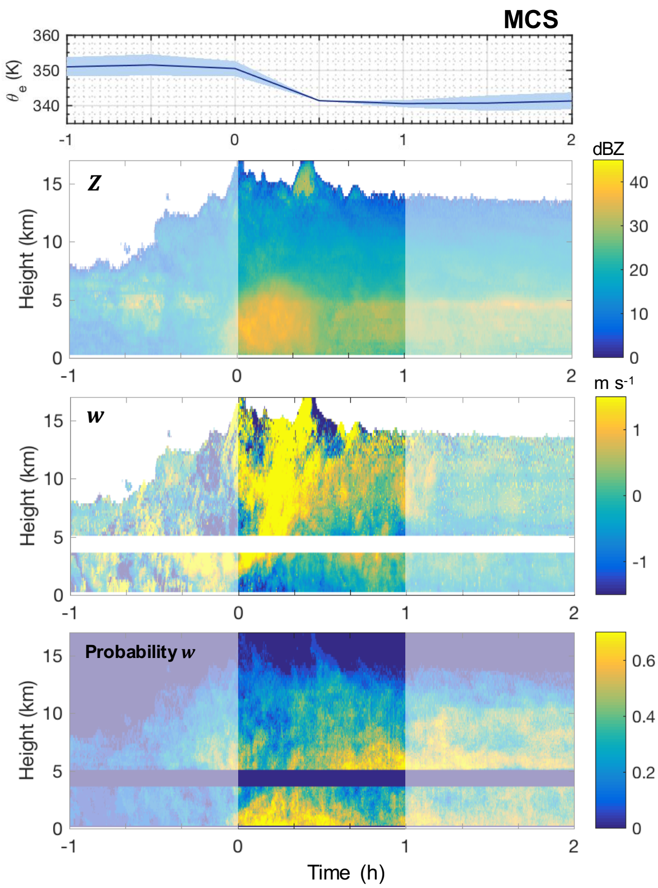

679
680 **Figure 6: Same as Fig. 5, but leading and lagging the passage of MCSs.**

681

Atmos. Chem. Phys. Discuss., https://doi.org/10.5194/acp-2017-684
Manuscript under review for journal Atmos. Chem. Phys.
Discussion started: 28 August 2017

Atmospheric Chemistry and Physics
Open Access
Discussions

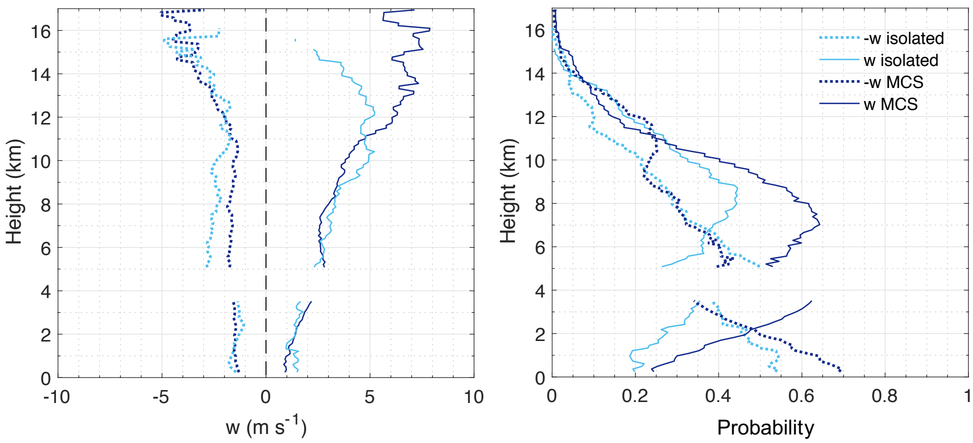

Figure 7: (left) Mean vertical velocity profiles for MCSs and isolated cells for downdrafts (w < 0 m s^{-1}; dashed) and updrafts (w > 0 m s^{-1}; solid). (right) Mean probability of observing updrafts or downdrafts as a function of altitude. Means are composited from data in the 30 minutes of largest drop in $\Delta\theta_e$ (0-0.5 h in Figs. 2, 3, 5, and 6).

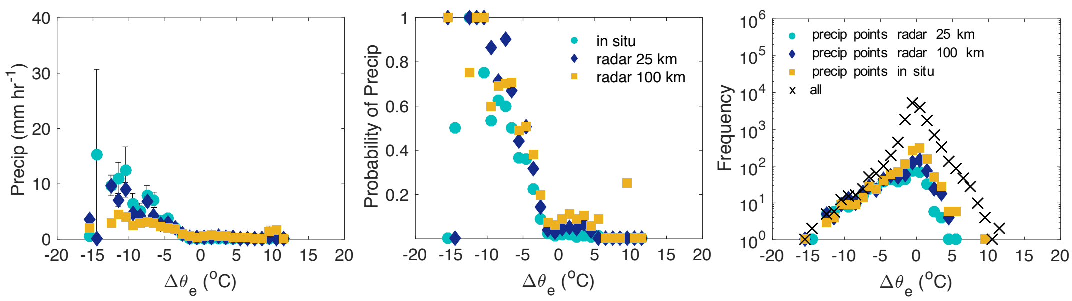

Figure 8: (left) Precipitation (30-min averages) conditionally averaged by coincident changes in equivalent potential temperature ($\Delta\theta_e$) at the GOAmazon site. Precipitation values corresponds to the θ_e values at the end of each differencing interval. Bins are a width of 1°. (middle) The probability of precipitation (> 1 mm h^{-1}) occurring for a given $\Delta\theta_e$. (right) The frequency of occurrence of $\Delta\theta_e$ and precipitation for a given $\Delta\theta_e$ (precip > 1 mm h^{-1}). Precipitation derived from S-Band radar reflectivity at spatial averages over 25 km and 100 km grid boxes surrounding the GOAmazon site are included for comparison to the in situ precipitation.

Atmos. Chem. Phys. Discuss., https://doi.org/10.5194/acp-2017-684
Manuscript under review for journal Atmos. Chem. Phys.
Discussion started: 28 August 2017

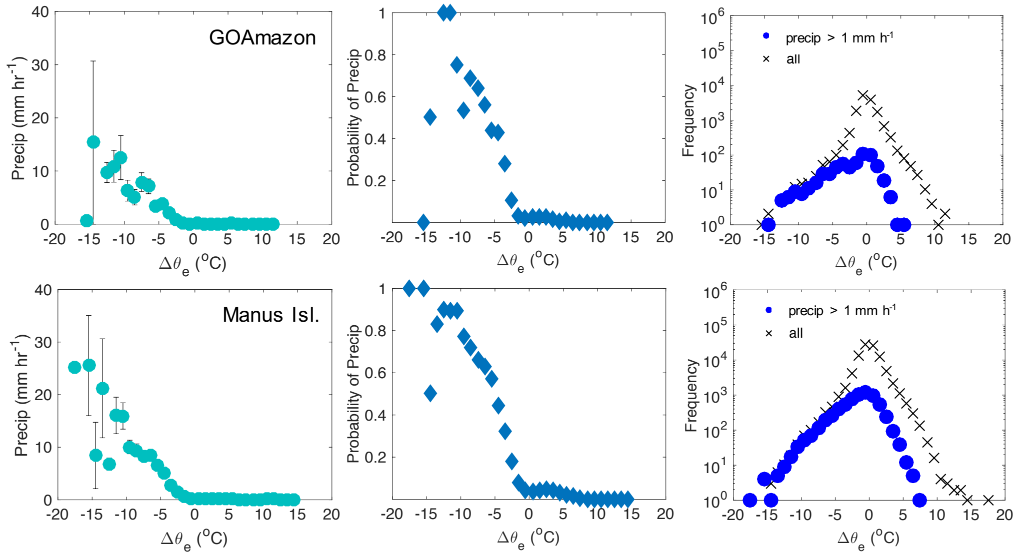

Figure 9: (left) Precipitation (30-min averages) conditionally averaged by coincident changes in equivalent potential temperature ($\Delta\boldsymbol{\theta_e}$) at the GOAmazon site (top) and Manus Island (bottom). Precipitation values corresponds to the $\boldsymbol{\theta_e}$ values at the end of each differencing interval. Bins are a width of 1°. (middle) The probability of precipitation occurring for a given $\Delta\boldsymbol{\theta_e}$. (right) The frequency of occurrence of $\Delta\boldsymbol{\theta_e}$ and precipitation for a given $\Delta\boldsymbol{\theta_e}$.

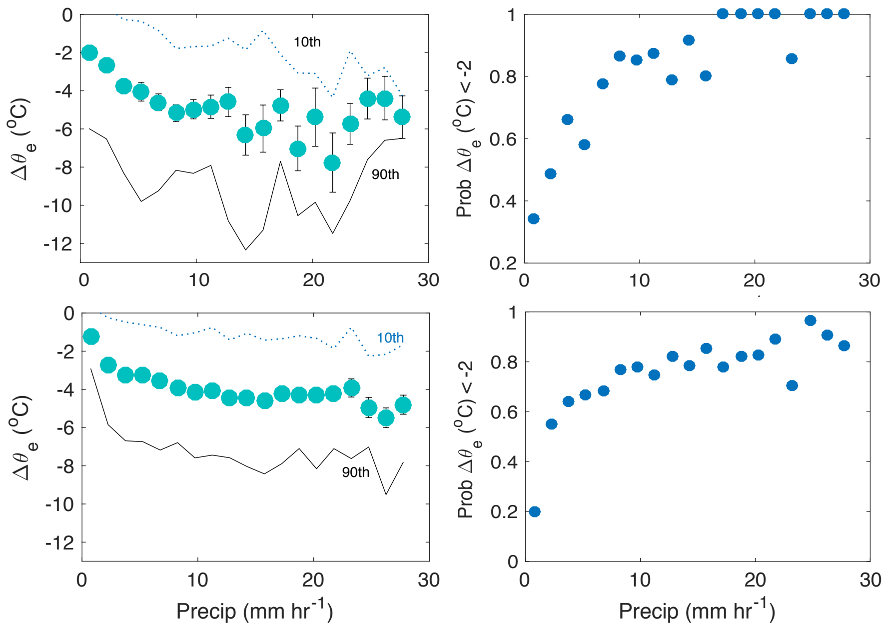

Figure 10: $\Delta\theta_e$ conditionally averaged by coincident precipitation (1-h averages) at the GOAmazon site (top) and at Manus Island (bottom). Precipitation values corresponds to the θ_e values at the end of each differencing interval. Bins are a width of 1°. Error bars represent standard error. The 10th and 90th percentile values for each bin are drawn for reference.